Roughness scaling in cyclical surface growth

Subhadip Raychaudhuri,[1] Yonathan Shapir,[1,2] David G. Foster,[2,3] and Jacob Jorne[2]
[1]*Department of Physics and Astronomy, University of Rochester, Rochester, New York 14627*
[2]*Department of Chemical Engineering, University of Rochester, Rochester, New York 14627*
[3]*Eastman Kodak Company, Rochester, New York 14650*
(Received 25 May 2001; published 22 October 2001)

The scaling behavior of cyclical growth (e.g., cycles of alternating deposition and desorption primary processes) is investigated theoretically and probed experimentally. The scaling approach to kinetic roughening is generalized to cyclical processes by substituting the number of cycles n for the time. The roughness is predicted to grow as n^{β} where β is the cyclical growth exponent. The roughness saturates to a value that scales with the system size L as L^{α}, where α is the cyclical roughness exponent. The relations between the cyclical exponents and the corresponding exponents of the primary processes are studied. Exact relations are found for cycles composed of primary linear processes. An approximate renormalization group approach is introduced to analyze nonlinear effects in the primary processes. The analytical results are backed by extensive numerical simulations of different pairs of primary processes, both linear and nonlinear. Experimentally, silver surfaces are grown by a cyclical process composed of electrodeposition followed by 50% electrodissolution. The roughness is found to increase as a power law of n, consistent with the scaling behavior anticipated theoretically. Potential applications of cyclical scaling include accelerated testing of rechargeable batteries and improved chemotherapeutic treatment of cancerous tumors.

DOI: 10.1103/PhysRevE.64.051604 PACS number(s): 68.35.Ct, 05.70.Ln, 68.43.Mn, 81.10.Aj

I. INTRODUCTION

From diffusion-limited aggregation to molecular beam epitaxy (MBE), kinetic models of growth and aggregation have attracted much attention [1–5] in the last two decades due to diverse interests in physics, biology, chemistry, and engineering. Kinetic roughening of nonequilibrium surface growth was of particular interest. Crystal growth, the growth of bacterial colonies, and the formation of clouds in the upper atmosphere [6] are all examples of nonequilibrium phenomena that grow self-affine rough surfaces. On a fundamental level, the surface growth problem is a paradigm for a class of problems in nonequilibrium statistical mechanics. One crucial aspect of this class is the signature of scale invariance and universality, very similar to those observed in equilibrium critical phenomena, or in nonlinear dynamical systems [7]. Early investigations focused primarily on the scaling behavior of the surface roughness [1–5]. More recently they have touched upon other aspects such as the distribution of the surface width [8,9], distributions of the height and the average height velocity [4,10,11], density of extrema [12], persistence [13], and maximal height [14].

Processes that generate rough surfaces can be divided into two classes: (i) growth processes (e.g., by deposition, absorption) where the surface grows by adding material; and (ii) recession processes (e.g., by erosion, dissolution, or desorption) where material is being taken off such that a rough surface is generated. Examples of class (i) include crystal growth [1–3], electroplating [15], and biological growth [1,2,5,16], which have been studied widely. Class (ii) includes chemical dissolution [17], and has received much less attention than the first class.

Self-affine surfaces generated by growth (or recession) can be described using scaling analysis of the surface roughness. In general, the surface is characterized by the height $h(\vec{r},t)$ appropriate to a $(\tilde{d}=d-1)$-dimensional substrate of linear size L. The width of the surface $W(L,t)$ at a time t is given by

$$W(L,t)=\langle[h(\vec{r},t)-\langle h(\vec{r},t)\rangle]^2\rangle^{1/2}, \tag{1}$$

where $\langle h(\vec{r},t)\rangle$ is the average height, which is linear in time $\langle h(\vec{r},t)\rangle=vt$, v being the average growth (or recession) velocity. The angular brackets $\langle\rangle$ denote an average over both lateral sites and the ensemble of surface configurations.

$W(L,t)$ scales as [18]

$$W(L,t)\sim L^{\alpha}f(L/\xi(t))\sim L^{\alpha}f(L/t^{1/z}), \tag{2}$$

where $\xi(t)\sim t^{1/z}$ is the lateral correlation length and f is the scaling function. For large time $t\gg L^z$

$$W\sim L^{\alpha},$$

while for $t\ll L^z$

$$W\sim t^{\beta},$$

where $\beta=\alpha/z$ is the growth exponent. The height-difference correlation function

$$\Delta(r,t)=\langle[h(\vec{r}_0+\vec{r},t)-h(\vec{r}_0,t)]^2\rangle, \tag{3}$$

obeys scaling similar to that of the roughness:

$$\Delta(r,t)\sim r^{2\alpha}f(r/\xi(t))\sim r^{2\alpha}f(r/t^{1/z}). \tag{4}$$

For $r\ll t^{1/z}$

$$\Delta\sim r^{2\alpha},$$

while for $r \gg t^{1/z}$

$$\Delta \sim t^{2\beta}.$$

The relation between the height-difference correlation function $\Delta(r,t)$ defined above and the equal-time height-height correlation function $C(r,t)=\langle h(\vec{r}_0+\vec{r},t)h(\vec{r}_0,t)\rangle$ is simple:

$$\Delta(r,t)=2[C(0,t)-C(r,t)]. \tag{5}$$

Dynamic scaling in Fourier space is studied in terms of the structure factor $S(\vec{q},t)=\langle h(\vec{q},t)h(-\vec{q},t)\rangle$, where $h(\vec{q},t)$ is the Fourier transform of the height $h(\vec{r},t)$. The scaling hypothesis Eq. (2) can be translated to the Fourier space such that

$$S(\vec{q},t)=q^{-d-2\alpha}g(q/t^{-1/z}). \tag{6}$$

The surface width W can be readily calculated from $S(\vec{q},t)$ using the relation $W^2(L,t)=(1/L^{\vec{d}})\Sigma_{\vec{q}}S(\vec{q},t)$. In the theoretical analysis of surface growth it is convenient to work in Fourier space and compute first the structure factor rather than the roughness W itself. Also, in some experiments the surface is probed by scattering processes which provide its structure factor.

All processes within the same universality class share the same critical exponents. Their continuum growth equations differ at most by terms that are rendered irrelevant by the renormalization group flow. The asymptotic continuum stochastic equations corresponding to different universality classes (indexed by $i=1,2,\ldots$) are of the form of a Langevin equation

$$\frac{\partial h(\vec{r},t)}{\partial t}=A_i\{h\}+\eta_i(\vec{r},t)+v_i, \tag{7}$$

where $A_i\{h\}$ is a local functional depending on the spatial derivatives of $h(\vec{r},t)$ and the noise $\eta_i(\vec{r},t)$ reflects the random fluctuations in the deposition process and satisfies $\langle \eta_i(\vec{r},t)\rangle=0$ and $\langle \eta_i(\vec{r}_1,t_1)\,\eta_i(\vec{r}_2,t_2)\rangle=2D_i\delta^{\vec{d}}(\vec{r}_1-\vec{r}_2)\,\delta(t_1-t_2)$. Some generic processes and their universality classes are reviewed later (Sec. III).

In the present paper we focus on cyclical processes in which deposition and desorption are occurring alternately. Examples of cyclical processes are abundant in nature and technological applications. A technologically important example is rechargeable batteries, where metal is electrodeposited on an electrode during the discharge, followed by partial electrochemical dissolution of this metal during recharging. In chemotherapy treatment of cancer the malignant cells are subjected to a recessive cyclical process.

The basic premise of our scaling approach to cyclical processes is that the number of cycles n should substitute for the time variable. So we propose for cyclical processes that the scaling relation of Eq. (1) be replaced with

$$W_c(L,n)\sim L^{\alpha}f_c(L/\xi_c(t))\sim L^{\alpha}f_c(L/n^{1/z}), \tag{8}$$

where $\xi_c \sim n^{1/z}$ is the correlation length and f_c is the cyclical scaling function. For large n, $n \gg L^z$,

$$W \sim L^{\alpha},$$

while for $n \ll L^z$

$$W \sim n^{\beta},$$

where $\beta=\alpha/z$ is the growth exponent.

The rest of the paper is organized as follows. The next Sec. II is devoted to our analytical analysis. We will prove that Eq. (8) for cyclical scaling holds asymptotically for linear processes. In addition we will show how to obtain the scaling exponents of the cyclic process, given those of the two primary processes. An approximate renormalization group RG approach is introduced to study nonlinear effects. Section III contains a brief review of the generic universality classes and their lattice algorithms. Then we introduce other algorithms to implement numerically different recession processes. The actual results of our simulation of cyclical processes are described in Sec. IV. In Sec. V the experimental findings from cyclical electrodeposition/dissolution of silver are discussed. Section VI contains the conclusions with a discussion of potential practical applications of the cyclical scaling approach. A short summary of some of the results was published in Ref. [19].

II. ANALYTICAL RESULTS

The analytical approaches are based on a stochastic equation, like Eq. (7), which describes the growth process. Thus, we begin by obtaining the stochastic equation of the cyclical process. The first primary process is denoted by $i=1$ and the second by $i=2$. The durations of the first and second processes are $T_1=pT$ and $T_2=(1-p)T$, respectively (p and $1-p$ are the fractional parts of the two processes). The total time period for one cycle is $T=T_1+T_2$. The cyclic growth equation in terms of the basic two processes can be expressed as

$$\frac{\partial h}{\partial t}=[a_1h+\eta_1+v_1]\Theta(p-f(t)) + [a_2h+\eta_2+v_2]\Theta(f(t)-p), \tag{9}$$

where $f(t)$ is defined as the fractional part of t/T and $\Theta(x)$ is the unit step function.

A. Linear primary processes: Exact calculation of $S_c(\vec{q},t)$

First we will consider cyclical processes for which both the primary processes are linear. For linear processes $A_i\{h\}=a_i(\vec{\nabla})h(\vec{r},t)$, where $a_i(\vec{\nabla})$ is a linear differential operator. Time reversal symmetry is obeyed in this case if the height is measured relative to the average height. The average height depends on the growth ($v_i>0$) and recession ($v_i<0$) nature

of the primary processes. In terms of the average velocity $v_c = pv_1 + (1-p)v_2$, it is given by

$$\langle h(\vec{r},t)\rangle/T = nv_c + v_1 f(t)\Theta(p-f(t)) + \{(v_1-v_2)p + v_2[f(t)]\}\Theta(f(t)-p). \tag{10}$$

The roughness is insensitive to the sign of v_i and hence will not distinguish between growth/growth and growth/recession cyclical processes as long as the basic processes remain linear.

For linear processes Langevin equations of the form of Eq. (7) are easily solved in Fourier space to yield (assuming spatial isotropy in the basal plane) the structure factor

$$S(q,t) = \exp\{-2a(q)t\}S(q,0) + \frac{D}{a(q)}\{1-\exp[-2a(q)t]\}, \tag{11}$$

where $S(q,0)$ is the structure factor at $t=0$, which contains the information about the initial roughness. During the nth cycle of cyclical growth, the structure factor $S_c(q,[(n-1)+p]T)$ generated by the first primary process (of duration $T_1 = pT$) is assigned as the initial condition for the second primary process. The second process lasts for $T_2 = (1-p)T$ to yield the structure factor $S_c(q,nT)$ of the cyclical process after n cycles. This is again used as the initial structure factor for the first process in the $(n+1)$th cycle.

During the first cycle, the structure factor after the completion of the first primary process becomes

$$S(q,T_1) = \exp\{-2\bar{a}_1\}S(q,0) + \frac{D_1}{a_1}[1-\exp(-2\bar{a}_1)], \tag{12}$$

where $\bar{a}_i = a_i(q)T_i$ was defined. This is the initial structure factor for the second primary process and after the first complete cycle we obtain

$$S(q,T_2) = \exp\{-2(\bar{a}_1+\bar{a}_2)\}S(q,0) + \exp\{-2\bar{a}_2\}\left\{\frac{D_1}{a_1}[1-\exp(-2\bar{a}_1)]\right\} + \frac{D_2}{a_2}[1-\exp(-2\bar{a}_2)], \tag{13}$$

where $S_c(q,T) \equiv S(q,T_2)$. Proceeding in this manner, we finally arrive at the structure factor $S_c(q,n) \equiv S(q,nT)$ of the cyclic growth after n cycles as a geometric series which can be readily summed to yield

$$S_c(q,n) = \exp\{-2\bar{a}_c n\}S(q,0) + \left[\frac{D_1}{a_1}\exp(-2\bar{a}_2)\{1-\exp(-2\bar{a}_1)\} + \frac{D_2}{a_2}\{1-\exp(-2\bar{a}_2)\}\right]\left[\frac{1-\exp(-2\bar{a}_c n)}{1-\exp(-2\bar{a}_c)}\right], \tag{14}$$

where $\bar{a}_c = a_c T$ with

$$a_c = [a_1 p + a_2(1-p)]. \tag{15}$$

In the scaling limit of small q, Eq. (14) for $S_c(q,n)$ reduces to

$$S_c(q,n) \sim \frac{D_c}{a_c(q)}\{1-\exp[-2a_c(q)Tn]\}, \tag{16}$$

with the effective noise strength for the cyclic process defined as

$$D_c = pD_1 + (1-p)D_2. \tag{17}$$

In terms of the effective parameters a_c and D_c, the above structure factor for the cyclical process resembles that of a generic linear growth process [see Eq. (11)] with the number of cycles n as the new time variable. Effectively the time is being coarse grained over a period of T by eliminating the high frequency ($>2\pi/T$) modes. Hence we can use the standard scaling analysis [Eq. (6)] of the structure factor to determine the scaling exponents in the case of cyclical growth.

After a large number of cycles n the interface width becomes saturated. In that limit, Eq. (15) becomes $S_c(q,n) \sim D_c/a_c(q)$. The roughness exponent of the cyclic process is determined by the $q \to 0$ divergence of $1/a_c(q)$. Since $a_i(q) \sim q^{z_i}$, it is the process with smaller z_i that dominates the asymptotic cyclical roughness, and the roughness exponent is given by $\alpha_c = \min(\alpha_1,\alpha_2) = \frac{1}{2}\{\min(z_1,z_2) - (d-1)\}$. The primary process with the *smaller* roughness imposes its roughness exponent on the combined cyclical process. The larger α_i appears as a correction to the scaling exponent. Whether or not it is the leading one depends on how its contribution compares with that of the subleading term in $a_i(q)$ of the dominating primary process. Note that a subleading term in $a_c(q)$ might affect the behavior on a smaller scale, if its amplitude is large. In that case, the leading behavior takes over only beyond a crossover length (at which both contributions are comparable). Since the amplitudes of a_1 and a_2 in $S_c(q,n)$ are proportional to p and $(1-p)$, respectively, the longer the nondominant process lasts, the larger is the crossover scale, as could be expected. However, although in $a_c(q)$ only the dominant $a_i(q)$ is important beyond this crossover scale, this is not the case for the effective noise correlator D_c, which is a scale independent constant in Eq. (16). Thus, the *amplitude* of the leading power-law roughness is determined by both the primary processes.

In the growing phase of the interface roughness, the dynamic exponent z will dictate the cyclical power law behavior. Since n is multiplied by $a_c = [a_1 p + a_2(1-p)]T$ in Eq.

(16) and $a_i(q) \sim q^{z_i}$, the process with smaller z_i will again dominate the cyclical dynamics in the $q \to 0$ asymptotic limit to yield $z_c = \min(z_1, z_2)$. Then for the initial cycles ($nT \ll L^z$) the surface width will scale as n^β, with $\beta_c = \alpha_c / z_c$. In essence, the scaling exponents of the cyclic growth will be identical to those of the primary process with the smaller z_i.

B. Coarse-graining approach: The cyclic propagator $G_c(\vec{r},t)$

In the previous section the structure factor $S_c(\vec{q},t)$ [and hence its Fourier transform (FT) $S_c(\vec{r},t)$] was obtained exactly. The same method of successive integration of the cyclical equation of motion may be applied to derive the cyclic propagator $G_c(\vec{r},t)$ [or its FT $G_c(\vec{q},t)$]. However, the expression is cumbersome and not very useful. Since we only need the long-time behavior, we will take a different route of coarse-graining the equation of motion such that the equation for time scales larger than T will be derived and $G_c(\vec{r},t)$ can be read from it. This will also provide a direct connection to the RG approach introduced in the next section to study the behavior of nonlinear systems.

Our starting point is Eq. (9), which we choose to integrate over one cycle, such that the remaining equation will be a difference equation between the average heights of two consecutive cycles. So assume we average Eq. (9) on time $t \in [nT,(n+1)T]$. The integral will be divided into integration over two intervals: interval (1) $[nT, nT+T_1]$ and interval (2) $[nT+T_1,(n+1)T]$. We define the average height in the nth cycle as

$$H(\vec{r},n) = \frac{1}{T}\int_n^{n+1} dt\, h(\vec{r},t). \tag{18}$$

Our goal is to obtain the equation of motion for $H(\vec{r},n)$ on time scales $t > T$. The FT of Eq. (9) is

$$\begin{aligned}\frac{\partial h(\vec{q},t)}{\partial t} &= [a_1(\vec{q})h(\vec{q},t) + \eta_1 + v_1]\Theta(p - f(t)) \\ &\quad + [a_2(\vec{q})\, h(\vec{q},t) + \eta_2 + v_2]\Theta(f(t) - p) \qquad (19)\\ &= a_c(\vec{q})h(\vec{q},t) + [\Delta a_1(\vec{q})\Theta(p - f(t)) \\ &\quad + \Delta a_2(\vec{q})\Theta(f(t) - p)]h(\vec{q},t) \\ &\quad + (\eta_1 + v_1)\Theta(p - f(t)) + (\eta_2 + v_2)\Theta(f(t-p)),\end{aligned}$$

where $\Delta a_1(\vec{q}) = a_1(\vec{q}) - a_c(\vec{q})$ and $\Delta a_2(\vec{q}) = a_2(\vec{q}) - a_c(\vec{q})$. Let us now integrate each of the terms over one cycle, beginning with the left-hand side:

$$\begin{aligned}\frac{1}{T}\int_n^{n+1} dt \frac{\partial h(\vec{q},t)}{\partial t} &= \frac{1}{T}[h(\vec{q},(n+1)T) - h(\vec{q},nT)] \\ &= \frac{1}{T}[H(\vec{q},n+1) - H(\vec{q},n)] \\ &\quad + \frac{1}{T}\{[h(\vec{q},(n+1)T) - H(\vec{q},n+1)] \\ &\quad - [h(\vec{q},nT) - H(\vec{q},n)]\}. \qquad (20)\end{aligned}$$

The first term can be expressed as $\Delta H(\vec{q},n)/T\Delta n$. The second term contains the differences between the height at the beginning of the cycle and its average over a cycle. This term thus reflects the behavior within each cycle and is thus irrelevant to the behavior on the coarse-grained scale and will be dropped. (Note that it will vanish asymptotically and it is irrelevant since in the continuum limit it features a second derivative with respect to t.)

The integration of the first term on the right-hand side yields

$$\frac{1}{T}\int_n^{n+1} a_c(\vec{q})h(\vec{q},t)dt = a_c(\vec{q})H(\vec{q},n). \tag{21}$$

Integrating the second term,

$$\begin{aligned}&\frac{1}{T}\int_n^{n+1} [\Delta a_1(\vec{q})\Theta(p - f(t)) + \Delta a_2(\vec{q})\Theta(f(t) - p)]h(\vec{q},t)dt \\ &= \frac{\Delta a_1(\vec{q})}{T}\int_n^{n+p} h(\vec{q},t)dt + \frac{\Delta a_2(\vec{q})}{T}\int_{n+p}^{n+1} h(\vec{q},t)dt \\ &= \Delta a_1(\vec{q})p\left\{\frac{1}{T_1}\int_n^{n+p} h(\vec{q},t)dt\right\} + \Delta a_2(\vec{q})(1-p)\left\{\frac{1}{T_2}\int_{n+p}^{n+1} h(\vec{q},t)dt\right\} \\ &= \Delta a_1(\vec{q})p\, H_1(\vec{q},n) + \Delta a_2(\vec{q})(1-p)H_2(\vec{q},n) \\ &= [\Delta a_1(\vec{q})p + \Delta a_2(\vec{q})(1-p)]H(\vec{q},n) + \{\Delta a_1(\vec{q})p[H_1(\vec{q},n) - H(\vec{q},n)] + \Delta a_2(\vec{q})(1-p)[H_2(\vec{q},n) - H(\vec{q},n)]\},\end{aligned} \tag{22}$$

where $H_1(\vec{q},n)$ and $H_2(\vec{q},n)$ are the average heights during the two primary processes respectively (on the nth cycle). Upon coarse graining,

$$\frac{1}{T}\int_n^{n+1}[\Delta a_1(\vec{q})\Theta(p-f(t))+\Delta a_2(\vec{q})\Theta(f(t)-p)]h(\vec{q},t)dt$$

$$=[\Delta a_1(\vec{q})p+\Delta a_2(\vec{q})(1-p)]H(\vec{q},n). \quad (23)$$

This term contains information on the structure factor within the cycle and must vanish in the coarse-grained equation, since a_c was chosen [Eq. (15)] such that

$$(a_1-a_c)p+(a_2-a_c)(1-p)=0. \quad (24)$$

The velocity term yields the average velocity

$$\frac{1}{T}\int_n^{n+1}dt[v_1\Theta(p-f(t))+v_2\Theta(f(t)-p)]=v_c. \quad (25)$$

The noises η are random variables and we define this coarse-grained term by

$$\eta_c(n)=\frac{1}{\sqrt{T}}\left[\int_n^{n+p}dt\ \eta_1(t)+\int_{n+p}^{n+1}dt\ \eta_2(t)\right]. \quad (26)$$

It obeys $\langle\eta_c(n)\rangle=0$ and $\langle\eta_c(n)\eta_c(m)\rangle=2D_c\delta_{nm}$, and D_c satisfies Eq. (17).

Collecting all the terms, the coarse-grained difference equation for $H(\vec{q},n)$ is

$$\frac{\Delta H(\vec{q},n)}{T\Delta n}=a_c(\vec{q})H(\vec{q},n)+\eta_c(\vec{q},n)+v_c. \quad (27)$$

For $n\gg 1$, the difference equation is equivalent to the corresponding differential equation $\Delta H/\Delta n\simeq\partial H/\partial n$.

The cyclical propagator may be read from this linear equation:

$$G_c(\vec{q},n-m)=\exp\{-a_c(\vec{q})(n-m)\}\Theta(n-m). \quad (28)$$

This propagator obeys the usual relation with the structure factor if n is treated as a continuous variable replacing the time t:

$$S_c(\vec{q},n)=\frac{D_c}{a_c(\vec{q})}[1-|G_c(\vec{q},n)|^2]. \quad (29)$$

C. Nonlinear primary processes

Stochastic nonlinear equations of this type can be analyzed using the perturbative dynamic RG approach [2,23]. We develop an approximate RG technique for cyclical processes with one or both the primary processes being nonlinear. The first step is to set aside (for the initial RG iterations) all the nonlinearities from the primary processes and take only the linear Langevin equations. We showed above how to solve for the structure factor of such cyclical processes and get an effective $S_c(q,n)$ [see Eq. (16)] of a noncyclic process. Similarly, we have shown in the previous subsection how to obtain the propagator $G_c(q,n)$ of the same effective linear, noncyclical process. The second step is to take the effective ''free'' propagator $G_c(q,n)$ and then add back all the nonlinear terms of the primary processes as perturbations. The bare couplings of the nonlinear terms are multiplied by p and $(1-p)$ to take into account the relative durations of the two primary processes. The third and the final step is to study the RG flow of the parameters and determine the fixed points of the transformations and hence the scaling exponents. This dynamic RG procedure is approximate in the sense that the initial flow of the couplings is shifted, but as long as the starting point is not close to a separatrix in the parameter space (i.e., a border line between basins of attraction of two different fixed points) this will not alter the ultimate fixed point of the RG flow.

The cyclical process might have only one nonlinear primary process with the nonlinear perturbation being relevant under RG transformations. Then the cyclical scaling exponents are given by the exponents of the nonlinear primary process. Otherwise, the nonlinear term turns out to be irrelevant with respect to the dominant linear term (present in the coarse-grained cyclic free propagator) of the other (linear) primary process, of which the scaling exponents control the cyclic growth.

Both the primary processes might contain nonlinear terms which are treated as perturbations to the free propagator as described above. In most cases, one of the nonlinear terms will make the other one irrelevant under the RG flow and the primary process containing the relevant nonlinearity will carry through its scaling exponents for the cyclical process. If both the nonlinear terms are relevant, then the possibility of new cyclical growth exponents (different from those of both primary processes) cannot be ruled out. A prime candidate for such behavior will be a cyclical process in $d=2+1$ in which one process has a relevant nonlinearity while the second process has a relevant anisotropy in the basal plane [20].

III. GROWTH MODELS AND UNIVERSALITY CLASSES

In this section we present a brief review of the basic models of kinetic growth. The discrete lattice models for simulations corresponding to each universality class are presented. We were able to generalize most of the lattice models for desorption processes (reverse of growth) to be used in absorption/desorption cycles. These desorption algorithms are described in detail.

A. Random deposition

This is the simplest of all possible growth processes. From a randomly chosen site above the surface, a particle falls vertically until it reaches the top of the column under it, whereupon it is deposited. In this case

$$A_{RD}=0.$$

The scaling exponents are $\beta=0.5$ in all dimensions, but α is not defined for this model because the interface roughness is never saturated.

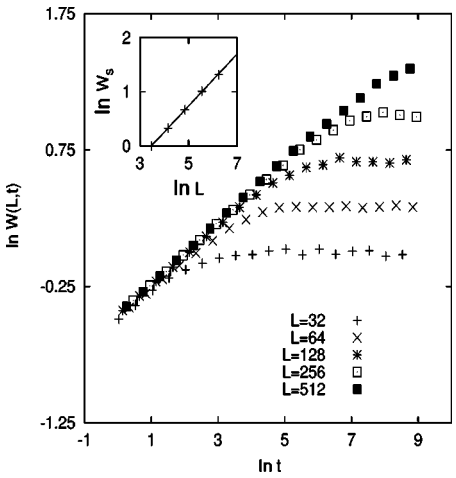

FIG. 1. The roughness W vs t in the EW desorption process (log-log plot). Inset: saturation roughness $\ln W_s$ vs $\ln L$.

The random deposition (RD) algorithm is as follows. A column i is chosen ($d=1+1$) randomly and its height $h(i,t)$ is increased by 1. For the reverse process we just decrease the height $h(i,t)$ of an arbitrarily chosen site i by 1.

B. Edwards-Wilkinson universality

In this model we have surface relaxation (in addition to the random deposition) which is introduced by the term

$$A_{EW}=\nu\nabla^2 h.$$

We can exactly calculate the scaling exponents $\alpha=(3-d)/2$, $\beta=(3-d)/4$, and $z=2$. In Edwards-Wilkinson (EW) growth [21] a randomly deposited particle can diffuse along the surface up to a finite distance and sticks to a local height minimum. Due to this relaxation, the surface becomes smooth compared to the random growth model and finally the interface roughness is saturated because of the correlations among the neighboring heights, to a value $\sim L^{\alpha}$, where L is the lateral size.

Family model

This model was introduced by Family [22] to simulate EW growth. A particle is dropped on a randomly chosen column i (in $d=1+1$) and sticks to the top of the column i, $i+1$, or $i-1$, depending on which of the three columns has the smallest height. To simulate a desorption process (with EW exponents), the height $h(i,t)$ of the site i is compared to the heights $h(i-1,t)$ and $h(i+1,t)$ of the neighboring sites. Then we simply take a particle off the column i, $i+1$, or $i-1$, depending on which of the three columns has the largest height. In the case of a tie involving the site i we take out a particle from that site, otherwise the tie is broken randomly with equal probability. The whole process can be thought of as desorption with surface relaxation. The relaxation length is restricted to the nearest neighbors because the scaling exponents are independent of the relaxation length. In Fig. 1 the roughness W is plotted against time on a logarithmic scale for increasing system size. The slope of the straight line fitted to the early time roughness yields the growth exponent $\beta=0.23\pm0.02$. The roughness exponent $\alpha=0.48\pm0.03$ is extracted from the dependence of the saturation roughness on the linear size of the system (inset of Fig. 1). These values of the scaling exponents are in agreement with the corresponding EW values. Indeed, the surface roughness for the desorption process shows (Fig. 1) very similar behavior to that obtained for the growth process [22]. So the discrete rules described above can be treated as a valid algorithm for EW desorption.

C. Kardar-Parisi-Zhang universality

This describes growth in a direction locally normal to the interface [23]. Its leading effect is to add a nonlinear term to the EW surface relaxation term,

$$A_{KPZ}=\nu\nabla^2 h+\frac{\lambda}{2}(\nabla h)^2.$$

Scaling exponents for the Kardar-Parisi-Zhang (KPZ) equation are exactly known in $d=1+1$: $\alpha=1/2$, $\beta=1/3$, and $z=3/2$. In $d=2+1$ approximate values for the exponents (from numerical simulations) are $\alpha\simeq0.39$, $\beta\simeq0.24$, and $z\simeq1.61$. KPZ growth can be simulated using various atomistic growth algorithms, of which we will describe two because we generalized those to the case of desorption and they will be used in our simulations of cyclical growth.

1. Ballistic deposition model

A particle is released from a randomly chosen position above the surface, located at a distance larger than the maximum height of the interface. The particle follows a straight vertical path until it reaches the surface, whereupon it sticks [24,25]. If $h(i,t)$ is the height of the column i (chosen randomly) at time t then the ballistic deposition (BD) growth rule is $h(i,t+1)=\max[h(i-1,t),h(i,t)+1,h(i+1,t)]$. For the reverse process the algorithm will be changed to $h(i,t+1)=\min[h(i-1,t),h(i,t)-1,h(i+1,t)]$. Although physically unrealistic (contrary to its growth counterpart) this desorption model is formally the ''anti-BD'' process.

2. Restricted solid-on-solid model

This algorithm (also known as the KK model) introduced by Kim and Kosterlitz [26] gives KPZ exponents and is known to yield reliable results even for small system sizes. The growth rule is to randomly select a site on a cubic $(d-1)$-dimensional lattice and to permit growth by letting the height of the interface $h_i\rightarrow h_i+1$ provided the restricted solid-on-solid (RSOS) condition on neighboring heights $|\Delta h|=0,1,\ldots,N (N\geqslant 1)$ is obeyed at all stages. In a similar way we can simulate an erosion process where we decrease the height ($h_i\rightarrow h_i-1$) of the site i provided the RSOS condition $|\Delta h|=0,1,\ldots,N$ is satisfied. In Fig. 2 we show the results of simulations using this desorption rule. The values of the scaling exponents ($\beta=0.33\pm0.02$ and $\alpha=0.52\pm0.02$) obtained are consistent with the corresponding KPZ values.

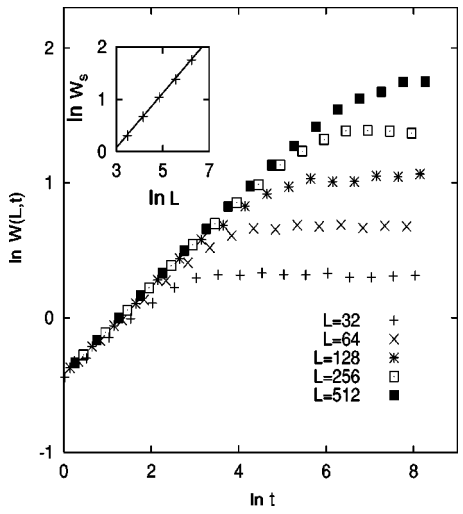

FIG. 2. The roughness W vs t in the KPZ (RSOS) desorption process (log-log plot). Inset: maximal roughness $\ln W_s$ vs $\ln L$.

The RSOS deposition or desorption rule described above is defined starting from a flat interface at $t=0$. A cyclical surface growth model with a primary process not obeying the RSOS condition can destroy the height difference restriction of the RSOS model. We can still use a growth rule similar to the RSOS model described above, which seems to behave like KPZ growth (as far as the scaling exponents are concerned). In this extended model of RSOS, we choose a site i randomly and add a particle on it only if the height of that site is less than or equal to the heights of the neighboring sites (which would give us the normal RSOS with $|\Delta h| = 0,1$ starting from a flat interface). For the reverse process a particle is taken off a site only if the height of that site is greater than or equal to the heights of the neighboring sites.

D. Mullins-Herring universality

In conserved growth situations where ''surface diffusion'' is dynamically significant in the absence of any EW relaxation process, the growth process may belong to the Mullins-Herring (MH) universality class [also known as the Das Sarma–Tamborenea (DT) or Wolf-Villain class] [27–29]. The linear surface diffusion equation for MH growth has a term

$$A_{MH} = -K\nabla^4 h.$$

The critical exponents for the MH growth universality are exactly known theoretically: $\alpha=(5-d)/2$, $\beta=(5-d)/8$, and $z=4$. In one dimension ($d=1+1$), the roughness exponent $\alpha=1.5$ exceeds unity, implying that the large scale steady state morphology of the growing interface is not self-affine in $d=1+1$. The issue of whether MH universality is only a crossover phenomenon or a true universality class is still debated [30]. There are two lattice models to simulate MH growth.

1. Das Sarma–Tamborenea model

In this model [28] a particle, after being deposited on a randomly chosen site, relaxes only to the nearest kink site, i.e., it seeks only to increase the number of neighbors.

2. Kim–Das Sarma model I

Choose a site i randomly and add a particle on $i-1$, i, or $i+1$ (in $d=1+1$), depending on which site has the largest curvature $\nabla^2 h=[h(x+1)+h(x-1)-2h(x)]$ [31]. If there is more than one site satisfying the larger curvature condition, we choose one among them randomly. If the curvature of the site i is one of the larger curvatures, we add the particle at site i.

E. Molecular beam epitaxy universality

The most relevant universality class in the context of conserved epitaxial growth is the molecular beam epitaxy universality [which also goes by the name Lai–Das Sarma–Villain universality] [32,33]. This is described by the nonlinear version of the MH surface diffusion equation with

$$A_{MBE} = -K\nabla^4 h + \lambda_1 \nabla^2 (\nabla h)^2.$$

The scaling exponents are known from a one-loop RG calculation which gives $\alpha=(5-d)/3$, $\beta=(5-d)/(7+d)$, and $z=(7+d)/3$. There are two discrete models to simulate the MBE universality class.

1. Lai–Das Sarma model

This model is similar to the DT model described above with the difference that if an atom falls in a kink site it is allowed to break its bonds and jump either down or up to the nearest kink site with the smallest step height [32].

2. Kim–Das Sarma model II

This is a generalization of the Kim–Das Sarma (KD) model I [31] described above. The only difference is that the linear curvature is replaced by a nonlinear curvature $[h(x-1)+h(x+1)-2h(x)]-(\lambda/2)\{[h(x-1)-h(x)]^2+[h(x+1)-h(x)]^2\}$.

IV. COMPUTER SIMULATIONS OF CYCLICAL GROWTH

A. Introduction

1. Simulation methods

To test our scaling hypothesis for cyclical processes we performed numerical simulations in $d=1+1$ using specific discrete growth models described above. The system size in the simulations was changed between 128 and 4096 lattice spacings. A periodic boundary condition is employed so that columns i and $i+L$ (L is the system size) are equivalent. A typical cycle consisted of a deposition of 5–20 layers (average number of particles deposited per site) and desorption of between 10% and 100% of the deposited amount. The maximum number of cycles n varied between 500 and 10 000 to reach saturation. To obtain good statistics we took an average over 50–5000 independent runs, depending on the pairs of primary processes and the system size. The smaller the system the larger was the number of runs to obtain good result.

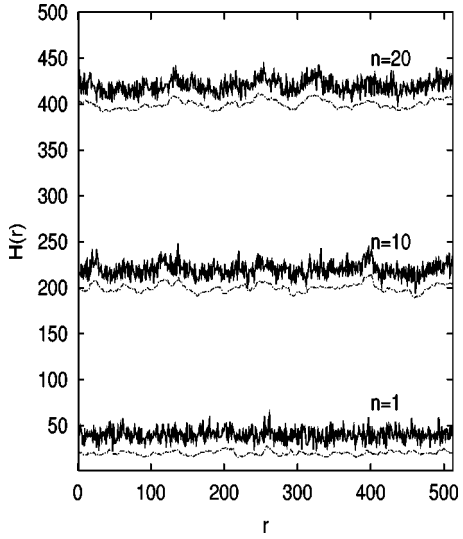

FIG. 3. Height profile for RD/EW cyclical growth. $L=512$ and 40 particles/site of random deposition (solid line) and 20 particles/site of EW dissolution (broken line) are used in one cycle (both axes are in lattice units).

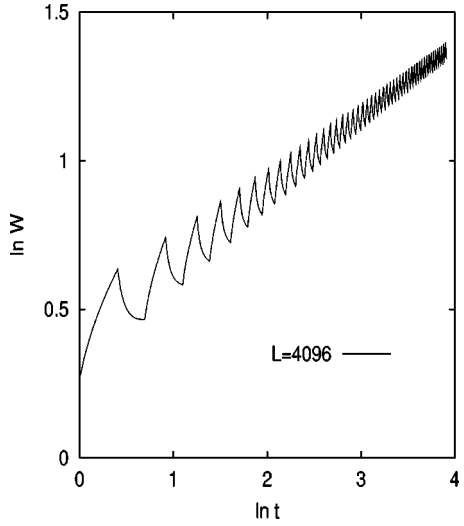

FIG. 4. $\ln W$ (roughness)$\sim \ln t$ of the MH/EW cyclic process. The DT process increases the roughness and EW smooths the surface in a single cycle, but the average roughness increases and gives rise to scaling (in terms of cycles).

2. Time dependence of surface roughness

In a single process of growth or desorption, the roughness scales with time [Eq. (2)]. For cycling, we have theoretically shown that time is replaced by a different scaling variable, the number of cycles n. One might ask: how does the cyclical roughness change with actual time leading to a scaling in terms of n? Below we discuss how the time (t) dependence of the surface roughness of cyclical growths can be studied to understand the emergent scaling behavior in terms of the number of cycles n.

Consider a linear growth (or erosion) process. The structure factor for this can be given by Eq. (11). From that expression of $S(q,t)$, the surface width $W^2=(1/L^{\tilde{d}})\Sigma_{\vec{q}}S(\vec{q},t)$ can be expressed as [34]

$$W^2(t)=W_0^2(t)+W_{flat}^2(t), \tag{30}$$

$W_{flat}(t)$ is the roughness for growth induced on a flat initial substrate, and W_0 is the contribution due to the width of the rough substrate surface. Since the total width is the sum of a decreasing (W_0) and an increasing (W_{flat}) part, competition between the two terms can make it increase or decrease from the initial roughness $W_0(0)$ for some time [eventually the roughness will exceed $W_0(0)$].

In cycling two primary processes act alternately. The roughness generated by one process is taken as the initial roughness $W_0(0)$ for the second process. In Fig. 3 the height profile is shown for cyclic growth with random deposition and EW desorption. EW dissolution smooths the very rough surface produced by random growth in one cycle. Also note that the roughness increases with the number of cycles n. In Fig. 4 we show the actual time dependence of the simulated cyclical growth composed of two linear primary processes belonging to the EW and MH universality classes. In one cycle, MH growth increases the surface width and then EW surface relaxation smooths out the surface to lessen the roughness. The average behavior of surface roughness in terms of cycles increases and gives rise to scaling. The scaling exponents are determined by the relevant (in the RG sense) terms of the primary processes. In our example (Fig. 4), MH/EW cycles are dominated by the surface relaxation of the EW model and the process gives rise to EW exponents. The change in roughness within a cycle can be thought of as fluctuations in the average behavior, and becomes less important as the number of cycles is increased (Fig. 4). Similar scaling (in terms of n) continues to hold for cyclic growth when one or both the primary processes are nonlinear.

3. Extraction of scaling exponents

The growth exponent β is extracted for different system sizes L. The roughness W vs n is plotted on a logarithmic scale and the slope of the best fitted straight line yields the exponent β. The value quoted is from the largest L (once the effective β became close to the asymptotic value). From $W_s(L)=W(L,\infty)$, the saturation width dependence on L, the roughness exponent α can be calculated. Simulation results for different system sizes are used to plot $\ln W_s \sim \ln L$, which is fitted to a straight line whose slope measures the exponent α. In some cases we checked independently the value of α from the scale dependence of the height-difference correlation function [from a log-log plot of $\Delta(r,t)$ vs r and fit to Eq. (4)].

B. Simulation results

1. Linear primary processes

For linear primary processes, we looked at the possible pairwise combinations of RD, EW, and MH universality classes using the absorption/desorption algorithms described earlier in this paper. When EW and MH processes are combined with RD, we obtain EW and MH exponents, respectively, because those are the processes that generate correlations on top of the random growth. Figure 5 shows, for the

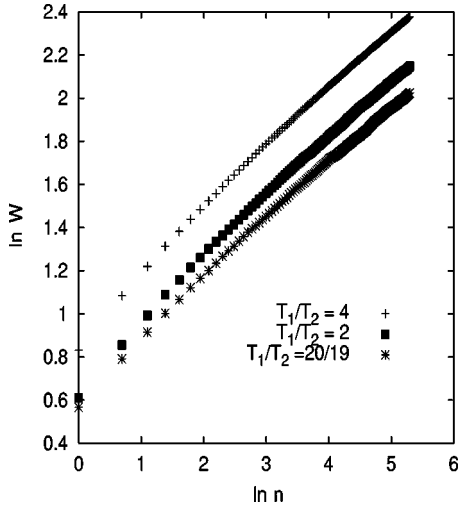

FIG. 5. The roughness W vs number of cycles n in RD/EW cyclical growth with different ratios of deposition T_1 and dissolution T_2 (log-log plot). System size $L=1024$ and deposition of 20 000 particles (fixed) are used.

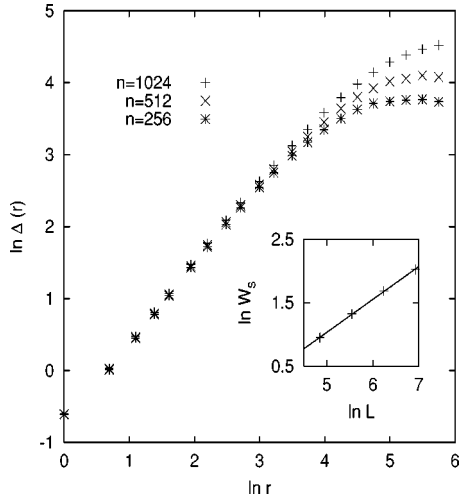

FIG. 7. Height-difference correlation function $\Delta(r)$ vs distance r for MH/EW cyclic growth is plotted after different number of cycles (log-log plot). Inset: $\ln W_s$ (maximal roughness calculated from Fig. 6) vs $\ln L$.

RD/EW cyclical process, that the value of β (asymptotically) is independent of the relative duration of the two primary processes. MH/EW cycles produce an asymptotic cyclical scaling with EW exponents $\beta=0.258(5)$ (Fig. 6) and $\alpha=0.52(3)$ (Fig. 7). We have also performed data collapse (Fig. 8) to establish the validity of our scaling hypothesis. The asymptotic EW exponents in MH/EW cycles confirm that the surface relaxation of EW is the dominating effect when paired with MH surface diffusion (or growth on kink sites). Our theoretical analysis also predicts that the EW scaling exponents will be imposed in the MH/EW cycles because EW growth has a smaller dynamic exponent ($z=2$) compared to that ($z=4$) of the MH universality class.

2. One nonlinear process with a linear one

To simulate nonlinear processes we used two lattice realizations BD and RSOS (with equivalent results) for the KPZ universality class and the KD II algorithm for MBE universality. First we combine the KPZ universality with the EW or MH universality in a cycle to see the effect of the nonlinear KPZ term on the scaling exponents. The exponents obtained are $\beta=0.311(5)$ and $\alpha=0.51(1)$ for EW/BD. The exponent β increased slowly with increasing system size and the effective β reached a value close to the asymptotic one only for the largest system size ($L=4096$). For the reverse process BD/EW we obtained $\beta=0.322(5)$ and $\alpha=0.50(1)$ (see Fig. 9). These asymptotic exponents are consistent with the KPZ $\beta=1/3$ and, of course, with $\alpha=1/2$, which is the common value of EW and KPZ. To look at primary processes with different values of α, KD I ($\alpha_1=1.5$) deposition with ballistic desorption ($\alpha_2=0.5$) was performed. We obtain the asymptotic values of the exponents for MH/KPZ, β

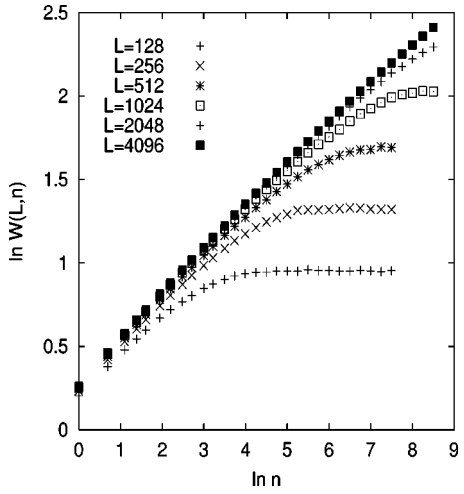

FIG. 6. $\ln W$ (roughness) vs $\ln n$ (number of cycles) of the MH/EW cyclical process for different system sizes L.

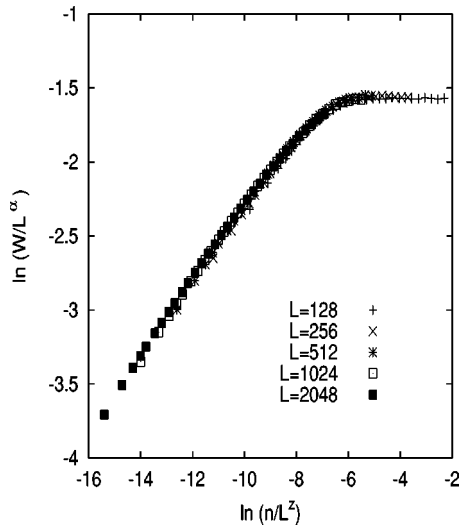

FIG. 8. Data collapse for MH/EW cyclical growth (using the exponents found from the graphs in Fig. 4 and Fig. 5) clearly shows scaling in terms of cycles n.

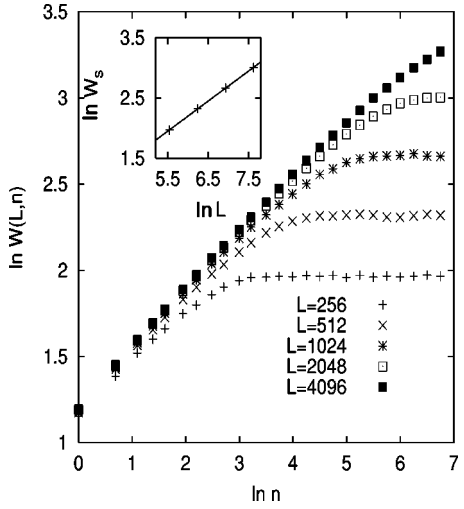

FIG. 9. ln W (roughness) vs ln n (number of cycles) of the simulated KPZ/EW cyclic growth for different system sizes L. Inset: roughness exponent α is extracted from the maximal values W_s for different L.

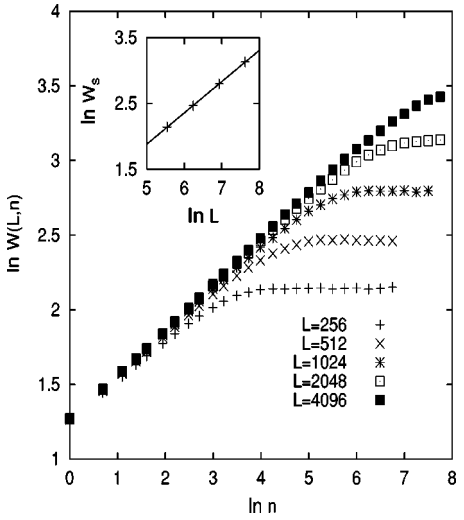

FIG. 10. The roughness W vs n of the KD II/BD (growth/growth) cyclical process (log-log plot). Inset: saturation roughness ln W_s vs ln L.

$=0.311(15)$ and $\alpha=0.48(2)$, both consistent with the KPZ values. In all these cyclic processes the KPZ nonlinearity $(\nabla h)^2$ remained relevant with respect to the linear terms ($\nabla^2 h$ or $\nabla^4 h$) and the growth retained its scaling exponents. To show the opposite behavior where the nonlinear process is not the dominant one we simulated MBE/EW cycles. From our approximate RG procedure for the cyclic process, it is clear that the fourth-order nonlinear perturbation $\nabla^2(\nabla h)^2$ is irrelevant with respect to the linear EW term $\nabla^2 h$. In our simulation, when we allow surface relaxation of the EW model only to the nearest neighbor we get an effective exponent ($\beta \approx 0.31$) different from the EW β even for the largest system size ($L=4096$) we used. The reason may be that the next nearest neighbors of a chosen site affect the curvature dependent growth process in the simulation of MBE. When we consider next nearest neighbors for surface relaxation in the EW process in MBE/EW cycles we get $\alpha=0.50(2)$ and $\beta=0.251(3)$, consistent with EW values.

3. Two nonlinear processes

Finally, we tried cycles consisting of two nonlinear primary processes belonging to the KPZ and MBE universality classes. Simulations of RSOS/RSOS (note that they are not time-reversed images of each other because of the nonlinearity) gave surfaces with KPZ scaling for $T_1 \neq T_2$. For $T_1 = T_2$, however, EW behavior was found. This follows from the nonlinear KPZ terms in the primary processes having the same magnitude but opposite signs. Hence, they exactly cancel each other in the coarse-grained growth equations, yielding an EW process. When we combine KPZ growth (using BD and KK) with MBE (KD II) we expect to get KPZ scaling for cycles due to the dominant KPZ nonlinearity (in $d=1+1$, where perturbative RG is applicable). Although both the processes have the same β (in $1+1$), in our simulation of cycles we observe a slow increase of β with increasing system size when the BD model is used to simulate KPZ growth. The value of the effective β for the largest system size ($L=8192$) did not reach the asymptotic value (1/3). Also, some sort of crossover behavior is observed, which varies depending on the ratio of T_1 and T_2. The BD model itself is not very efficient to reach the asymptotic regime of KPZ growth and probably that is reflected in the simulations of cyclical growth. When we used the RSOS model for the KPZ part of the cycle, the asymptotic scaling exponents [$\alpha=0.50(1)$ and $\beta=0.335(5)$] were obtained for relatively small system sizes.

We also ran the corresponding absorption/absorption (or growth/growth) cycles with identical roughness behavior. Figure 10 shows the results of a KD II/BD growth/growth cycling simulation. The scaling exponents [$\beta=0.31(2)$ and $\alpha=0.48(2)$] again acquire the corresponding KPZ values as expected.

V. EXPERIMENTS ON CYCLIC GROWTH

Experiments of cyclical growth were performed by metal electrodeposition/dissolution of silver. The scaling behavior of surface roughness has been studied for electrochemical deposition [15,35–37] and dissolution [17] processes separately. In cycling, however, metal electrodeposition followed by a partial dissolution occurs. The substrate is plated for a specific period of time and then the current is reversed and the metal is dissolved from the substrate. This phenomenon is inherent in rechargeable batteries.

Multiple cycles were carried out on vapor-deposited silver substrates, ranging from 1 to 20 cycles. The plating solution contained $0.092M$ AgBr (silver bromide), $0.23M$ $(NH_4)_2S_2O_3$ (ammonium thiosulfate), and $0.17M$ $(NH_4)_2SO_3$ (ammonium sulfite). Each cycle consisted of plating for 5 min followed by 2.5 min of electrodissolution with a current density of 0.8 mA/cm^2. Image and scaling analysis was done using an atomic force microscope. Roughness was measured after n full cycles and after the deposition part of the cycles (i.e., after $n+p$ cycles with

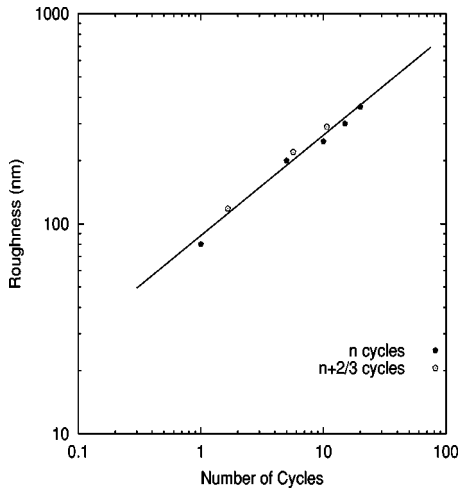

FIG. 11. The roughness vs number of cycles n in the electrochemical cyclical growth of silver (log-log plot).

$p=2/3$). A logarithmic plot of saturation rms height versus number of cycles, shown in Fig. 11, resulted in a straight line over two decades, indicating that the roughness scales with the number of cycles n, with $\beta=0.52$, where β is the growth exponent. The roughness for cycling and deposition alone is compared. The value of β is 0.52 for the cycling processes and 0.62 for deposition alone [38], suggesting that processes such as the erosion of rough areas and the filling in of surface recesses are occurring more during cycling than in straight deposition. However, the saturation rms height was larger in magnitude for cycling than for straight deposition.

The results suggest that cycling causes smoothing of the surface recesses and valleys by the dissolution of large peaks during the reverse plating process.

VI. CONCLUSIONS

In this paper we have discussed *cyclical* growth processes using dynamic scaling in terms of the number of cycles n (replacing the time variable t of simple growth). Given two primary processes we have described how to derive the scaling exponents of the combined cyclical process. Monte Carlo simulations of different cyclic processes were carried out using various simple pairs of primary growth processes. The results of numerical simulations are entirely consistent with our theoretical understanding. For linear processes, the primary process with smaller dynamic exponent z always imposes its own scaling exponents on the combined cyclical process. The application of the RG method to cyclical processes was presented to determine cyclical scaling exponents in the case of nonlinear primary processes. In particular, cyclical scaling exponents are independent of the relative duration (p or $1-p$) of the primary process and also of the duration T of the cycle. However, both p and T do affect the amplitude of the roughness and also the crossover length beyond which the asymptotic exponents show up. Experimental results on electrodeposition-dissolution cycles are in accordance with our scaling hypothesis.

Cyclic growth phenomena are widespread in nature: the sea shores are shaped by cyclical high and low tides associated with lunar motion around the Earth, all floral growth is subjected to daily changes in light and seasonal variations (which also affect many geological processes), etc. Thus the cyclical scaling theory introduced here might be found helpful in future investigations of many natural growth phenomena.

Cyclical processes are also ubiquitous in technological applications. For example, corrosion processes are strongly affected by seasonal weather conditions. The most likely application of our theory is for rechargeable batteries. Indeed, one of the breakdown mechanisms is due to the metal grown on one electrode reaching the other one, thereby causing a shortcircuit. To test batteries today one has to run them for their full lifetime. Using cyclical scaling, however, accelerated testing will become feasible. Results from measurements on fewer cycles for a short amount of time could be extrapolated to predict the battery lifetime under its realistic working conditions.

Finally, application to medicine may also be envisioned. The first one that comes to mind is the treatment of malignant tumors. They are known to have rough surfaces which follow the kinetic growth scaling laws [16]. Under chemotherapeutic (or radiation) treatment they shrink and, hopefully, disappear. These treatments are always cyclical, and thus the cyclical scaling approach should faithfully describe the tumor's recession. We hope that using this approach will help plan the schedule and dosage of the treatments so as to make them more efficient while minimizing the side effects.

ACKNOWLEDGMENTS

One of us (S.R.) is grateful to S. Raghavan for his help in using the software XFIG. This work was supported by the ONR Grant No. N00014-00-1-0057 and by the Eastman Kodak Company.

[1] *Dynamics of Fractal Surfaces*, edited by F. Family and T. Vicsek (Cambridge University Press, Cambridge, England, 1990).

[2] A.-L. Barabasi and H. E. Stanley, *Fractal Concepts in Surface Growth* (Cambridge University Press, Cambridge, England, 1995).

[3] J. Villain and A. Pimpinelli, *Physique de la Croissance Crystalline* (Editions Eyrolles, Paris, 1995).

[4] T. Halpin-Healy and Y.-C. Zhang, Phys. Rep. **254**, 215 (1995).

[5] P. Meakin, *Fractals, Scaling and Growth Far from Equilibrium* (Cambridge University Press, Cambridge, England, 1998).

[6] J. D. Pelletier, Phys. Rev. Lett. **78**, 2672 (1997).

[7] J. M. Burgers, *The Nonlinear Diffusion Equation: Asymptotic Solutions and Statistical Problems* (Riedel, Boston, 1974).

[8] G. Foltin, K. Oerding, Z. Racz, R. L. Workman, and R. K. P.

Zia, Phys. Rev. E **50**, R639 (1994).
[9] Zoltan Racz and Michael Plischke, Phys. Rev. E **50**, 3530 (1994).
[10] J. M. Kim, M. A. Moore, and A. J. Bray, Phys. Rev. A **44**, 2345 (1991).
[11] B. Derrida and J. L. Lebowitz, Phys. Rev. Lett. **80**, 209 (1998); B. Derrida and C. Apert, J. Stat. Phys. **94**, 1 (1999).
[12] Z. Toroczkai, G. Korniss, S. Das Sarma, and R. K. P. Zia, Phys. Rev. E **62**, 276 (2000).
[13] Z. Toroczkai and E. D. Williams, Phys. Today **52** (12), 24 (1999); J. Krug *et al.*, Phys. Rev. E **56**, 2702 (1997); H. Kallabis and J. Krug, e-print cond-mat/9809241; S. N. Majumdar, Curr. Sci. **77**, 370 (1999).
[14] S. Raychaudhuri, M. Cranston, C. Przybyla, and Y. Shapir, Phys. Rev. Lett. **87**, 136101 (2001).
[15] A. Iwamoto, T. Yoshinobu, and H. Iwasaki, Phys. Rev. Lett. **72**, 4025 (1994).
[16] A. Bru *et al.*, Phys. Rev. Lett. **81**, 4008 (1998).
[17] A. Iwamoto, T. Yoshinobu, and H. Iwasaki, Phys. Rev. E **59**, 5133 (1999).
[18] F. Family and T. Vicsek, J. Phys. A **18**, L75 (1985).
[19] Y. Shapir, S. Raychaudhuri, D. G. Foster, and J. Jorne, Phys. Rev. Lett. **84**, 3029 (2000).
[20] M. Kardar, in *Dynamics of Fluctuating Interfaces and Related Phenomena*, edited by D. Kim, H. Park, and B. Kahng (World Scientific, Singapore, 1997), p. 30; B. Kahng, *ibid.*, p. 67.
[21] S. F. Edwards and D. R. Wilkinson, Proc. R. Soc. London, Ser. A **381**, 17 (1982).
[22] F. Family, J. Phys. A **19**, L441 (1986).
[23] M. Kardar, G. Parisi, and Y.-C. Zhang, Phys. Rev. Lett. **56**, 889 (1986).
[24] M. J. Vold, J. Colloid Sci. **14**, 168 (1959).
[25] P. Meakin, P. Ramanlal, L. M. Sander, and R. C. Ball, Phys. Rev. A **34**, 5091 (1986).
[26] J. M. Kim and J. M. Kosterlitz, Phys. Rev. Lett. **62**, 2289 (1989).
[27] W. W. Mullins, J. Appl. Phys. **28**, 333 (1957); C. Herring, *ibid.* **21**, 301 (1950).
[28] S. Das Sarma and P. Tamborenea, Phys. Rev. Lett. **66**, 325 (1991).
[29] D. E. Wolf and J. Villain, Europhys. Lett. **13**, 389 (1990).
[30] S. Das Sarma, e-print cond-mat/9705118, and references therein.
[31] J. M. Kim and S. Das Sarma, Phys. Rev. Lett. **72**, 2903 (1994).
[32] Z. W. Lai and S. Das Sarma, Phys. Rev. Lett. **66**, 2348 (1991).
[33] J. Villain, J. Phys. I **1**, 19 (1991).
[34] S. Majaniemi, T. Ala-Nissila, and J. Krug, Phys. Rev. B **53**, 8071 (1996); J. Krug, Adv. Phys. **46**, 139 (1997).
[35] G. L. M. K. S. Kahanda, X. Zou, R. Farrel, and P. Wong, Phys. Rev. Lett. **68**, 3741 (1992).
[36] W. M. Tong and R. S. Williams, Annu. Rev. Phys. Chem. **45**, 401 (1994).
[37] W. U. Schmidt, R. C. Alkire, and A. A. Gewirth, J. Electrochem. Soc. **143**, 3122 (1996).
[38] D. G. Foster, Ph.D. thesis, University of Rochester, 1999; D. G. Foster, J. Jorne, Y. Shapir, and S. Raychaudhuri (unpublished).